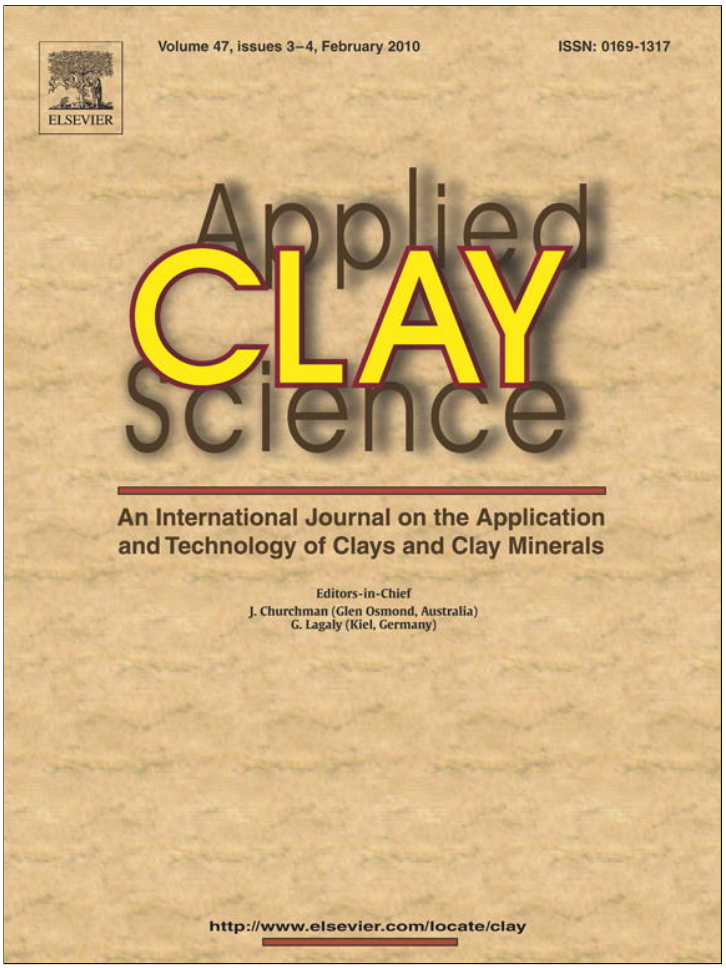

Applied Clay Science 47 (2010) 290–302

Contents lists available at ScienceDirect

Applied Clay Science

journal homepage: www.elsevier.com/locate/clay

Genesis of the La Espingarda kaolin deposit in Patagonia

Eduardo A. Domínguez [a,*], Claudio Iglesias [b], Michele Dondi [c], Haydn H. Murray [d]

[a] Departamento de Geología, Universidad Nacional del Sur, San Juan 670, 8000 Bahía Blanca, Argentina
[b] Piedra Grande SA, Dique Florentino Ameghino, Dto. Gaiman, A.P. Bell 569, 9100 Trelew, Chubut, Argentina
[c] CNR-ISTEC, Istituto di Scienza e Tecnologia dei Materiali Ceramici, Via Granarolo 64, 48018 Faenza, Italy
[d] Indiana University, Dept. Of Geological Sciences, 1001 E. Tenth St., Bloomington, IN 47405, United States

ARTICLE INFO

Article history:
Received 16 December 2008
Received in revised form 10 November 2009
Accepted 16 November 2009
Available online 26 November 2009

Keywords:
Kaolin
Genesis
Epithermal
Exploration

ABSTRACT

The La Espingarda kaolin deposit was formed by "in situ" alteration of sub-alkaline rhyolites belonging to the Jurassic Marifil Formation. Three altered volcanic lithofacies were identified: a porphyric biotitic ignimbrite (RPB), a coarse lithic ignimbrite (ILG), and a fluidal intrusive rhyolite (RFI).

The kaolinization covers an ellipsoidal surface area of ~20,000 m^2, with the alteration intensity decreasing downwards and disappearing at 8–12 m from the surface. In two mine sectors small stockworks of fine quartz veins appears (<3 m^2). The deepest alteration is related to two fault zones where the three volcanic units are in contact. There is no lateral clay zoning at the faults. The mineralogical composition is kaolinite ± halloysite ± illite + quartz + feldspars + Fe-hydr(oxides). At least three kaolinite generations were identified. The first is pervasive; the second appears as a filling of vugs in the quartz veinlets that crosscut the pervasively altered rocks; and the third occurs as pure kaolin veins without quartz vein cross cuts. During the alteration processes almost total alkali cations were leached. The argillized lithofacies showed Ni enrichment and Cu, Sr, and Ba depletions.

The main weathering genesis for La Espingarda is supported by the deposit morphology, its location in topographic lows, the paleoclimatic record, its simple mineralogical composition; vertical zonation, the kaolinite veins isotopes ($\delta^{18}O$ ‰ 18.3; δD ‰ −59.0), and the trace element distribution.

A steam heated water activity produced some kaolinite overprint according to one isotopic value and the S and P contents slightly higher in the kaolinized rocks. Neither Au, Ag, As, Sb, Hg, or Ba epithermal pathfinders' anomalies nor drill data support the existence of any metallic mineralization at the kaolin blanket bottom.

In Patagonia hydrothermal kaolinite manifestations are located around and beneath silicified, erosion-resistant hills and include some of the following minerals: dickite, alunite, pyrophyllite, or pyrite and have As, S, Ba, and Ag trace elements within the range of weak geochemical anomalies.

1. Introduction

In Patagonia, Southern Argentina, there is an extended Triassic–Jurassic Gondwana Rhyolite Province that contains primary kaolin and epithermal gold deposits (Schalamuk et al., 1997; Domínguez and Cravero, 1999; Sotarello et al., 2002; Sillitoe, 2004; Rubinstein and Gargiulo, 2005). The rocks of this Gondwana Rhyolite Province have different regional names, being the Marifil Formation (Malvicini and Llambias, 1974) at the deposit area.

These rhyolites contain numerous primary kaolin deposits that supply clays to the ceramic industry. The main deposits are located along the Lower Valley of the Chubut River, although some others as Lote 8, Cº Rubio, Blanquita and Equivocada, are also important. There are also secondary "Ball Clay"-type kaolin layers in younger sedimentary sequences linked to them. The rhyolites also contain numerous epithermal gold deposits some of which are at present under or will be in exploitation in the near future such as Cerro Vanguardia (Zubia et al., 1999); Veta Martha (González Guillot et al., 2004), Huevos Verdes, Manantial Espejo, and Esquel (Sillitoe et al., 2002) among others.

This work focuses on the study of the geology and genesis of "La Espingarda" kaolin deposit located near Dique Ameghino, in Chubut Province. This mine presents an excellent opportunity for a geologic–genetic study because it is in a mature production stage having several exposed mine faces and drilling records that allow a detailed alteration study. Three lithofacies have been altered and each one has its own kaolinite identity. In the deposit, new observations and careful detailed determinations indicate that weathering was the principal kaolinite formation environment.

Since kaolinite can form under weathering or hydrothermal conditions, it is important to distinguish its genesis because, in the last case, the kaolinite manifestations are blankets for precious metal deposit exploration (Bethke, 1984; Hedenquist et al., 2000). Recently, the kaolinite halo

* Corresponding author. Tel.: +54 291 4595100 Int 3065; fax: +54 291 4595140.
E-mail address: edomin@criba.edu.ar (E.A. Domínguez).

0169-1317/$ – see front matter © 2009 Elsevier B.V. All rights reserved.
doi:10.1016/j.clay.2009.11.030

in the Blanquita, Equivocada and C° La Mina deposits have been confirmed to be hydrothermal (Marfil et al., 2005; Ducart et al., 2006).

Faced with this evidence, the idea of a genetic relation between residual kaolinites and epithermal deposits is once again being considered. This study shows that the kaolinite blanket at "La Espingarda" and others with similar geology do not have any exploration potential for precious metal discovery.

The origin of primary kaolin deposits in Patagonia has been a topic of scientific discussion for a long time: Angelelli and Stegman (1948) and Oliveri and Terrero (1954) found evidence that supports a weathering origin, but Hayase (1969) and Maiza and Hayase (1975) proposed that such deposits were formed by hydrothermal fluids. Romero et al. (1975) linked the genesis to underground water circulation and Logan et al. (1992) concluded that they were formed by hydrothermal fluids without discarding overimposed weathering. Based on isotopic determinations, Domínguez and Murray (1995) attributed the genesis of kaolin to weathering conditions, although restricted hydrothermal influences could not be ruled out.

2. Regional geology

Major Argentinean primary kaolin deposits are located in the lower valley of the Chubut river. Along the valley there are more than 400 kaolin mines that provide about 60% of the country's total production (i.e. 60,000 tons/year). The mines are located between Dolavon and Dique Ameghino embracing an area of 2500 km^2, being one of the deposits of La Espingarda (9000 tons/year) that has more faces exposed to study its geology.

The lower valley of the Chubut River is located south of the Macizo de Somuncura (Stipanicic and Methol, 1972) and its geology is characterized by a Proterozoic metamorphic basement intruded by Permo-Ordovician granites that are covered extensively by the rhyolitic vulcanites from the Marifil Fm according to Sacomani and Panza (1998) (Fig. 1).

Major outcrops at La Espingarda are rhyolitic ignimbrites, lava flows, and tuffs. Besides the prevalence of rhyolite, geochemical studies reflect a wide rock composition embracing the whole rhyolite-basalt series (Uliana et al., 1985). The rhyolites were formed during Lower to Middle Jurassic time based on K–Ar radiometric ages of 158–210 Ma (Rapela and Pankhurst, 1993; Page et al., 1999). All the primary kaolin deposits appear along a regional discordance worked on the rhyolites overlaid by the younger sedimentary rocks.

Cretaceous continental deposits of the Chubut Group and the Danian Salamanca Fm marine sandstones with kaolinite layers, unconformably cover the rhyolitic vulcanites (Lesta and Ferello, 1972). In both cases the paleontological records indicate warm and humid climates (Bertels, 1973; Malumián, 1983; Pothe de Baldis, 1984). The Eocene Río Chico Fm (Simpson, 1933), the Eocene–Oligocene Sarmiento Fm (Spalletti and Mazzoni, 1977), the Upper Pliocene Montemayor Fm (Yllanes, 1979), and the Rodados Patagónicos (Windhausen, 1921) complete the stratigraphic column.

The oldest tectonic activity registered in this area corresponds to basement fissures that facilitated volcanic Jurassic spills during the Gondwana initial separation steps. The fissure formation was prior to the opening of the Atlantic Ocean and the volcanic processes are closely tied to this event (Ramos and Pesce, 1979). Blocks limited by faults are the dominant structural feature in this region which affects the Marifil Fm in a significant way.

3. Materials and methods

The kaolin deposit morphology was defined using geological field methods and the results of 84 holes totaling 503 m of drilling. The drill grid was approximately 25 m and the hole was finished when the sludge turned into fresh rock.

The petrographic, mineralogical, X-ray and chemical analyses comparing fresh, intermediate, and highly altered rocks were performed on typical point samples of each lithological unit (>10 samples).

Clay mineralogical composition was investigated on the point samples and also on a bulk mining sample (>80 kg) of each lithological unit by X-ray powder diffraction performed on both whole rock and <2 μm fractions randomly oriented using a Rigaku-Denki Geigerflex Max III C diffractometer ($2°2\theta\ min^{-1}$, graphite-monochromated Cu K_α radiation). The mineralogical composition was confirmed by its response to the glycolation-heated treatments on the oriented samples. The quantitative mineralogical composition was achieved using both normative calculations and X-ray pattern interpretation applying the generalized reference intensity ratio (RIR) and assuming a theoretical composition for kaolinite, quartz, and feldspars as well as a mean composition for illite. The kaolinite crystallinity was determined on <2 μm fraction obtained by washing, following the method proposed by Hinckley (1963). Because quartz is always present, even in <2 μm fractions, the Stoch index (Stoch, 1974) was used as recommended by Aparicio and Galán (1999). Clay microstructure was observed by scanning electron microscopy (SEM, JEOL 35 CF) using small fragments mounted on Cu holders and coated with an Au–Pd alloy. The halloysite presence was suspected by the X-ray pattern and was confirmed by its tabular morphology on SEM–TEM images of the bulk samples. Its abundance was estimated from the images.

Chemical analyses of major, minor and trace elements (including REE) were performed also at ACTLABS — Canada by Instrumental Neutron Activation Analysis (INAA), Inductively-Coupled Plasma Optical Emission Spectrometry (ICP-OES), and X-ray Fluorescence Spectrometry (XRF). Carbon and sulphur concentrations were determined by IR absorption (Leco CS225, ASTM E 1019).

Fluid inclusions were studied in the quartz veins. Micro thermometric measurements were carried out using doubly-polished wafers of 100–300 μm on a Linkam heating–freezing stage with a −180 to 600 °C working range mounted on an Olympus BX50 microscope with ×10–×25 oculars and UTK50/0.63 Leitz objectives. Calibration was obtained with standards in the 400 °C range, and with CO_2 and pure H_2O for freezing. The salinity of fluid inclusions was determined from the final melting temperature of ice (Tm) using Bodnar's equation (Bodnar, 1992).

The kaolinite isotopic analyses were performed on pure <2 μm samples at Actlabs — Canada (Protocol N° 21188D). The procedures of Clayton and Mayeda (1963) were used for O extraction. The D^{18} extraction was made at 1400 °C in platinum crucibles and the water reacted with U for the H acquisition. A Finnigan Spectrometer was used.

4. Deposit geology

The kaolinized area is found at the bottom of a small valley (Figs. 2 and 3) and in the quarry the dominant outcrops correspond to the flows, ignimbrites, and tuffs of the Marifil Fm. Resistant sandstones of the Salamanca Fm protected the soft kaolinized rocks.

In the volcanic complex four different lithofacies were recognized and described as porphyric biotite ignimbrite (RPB), coarse lithic ignimbrite (ILG), intrusive rhyolitic flow (RF), and fall tuffs (FT).

RPB ignimbrite is reddish with porphyric textures and, in hand samples, fractured angular quartz crystals, feldspars and subordinate biotite in a glassy re-crystallized groundmass were observed. Glassy shards without fluidal evidence were observed under the microscope. Texturally, it is a massive highly cohesive non-welded ignimbrite (Fig. 4).

ILG ignimbrite is pinkish when fresh and yellowish-brown on weathered surfaces. It is a massive lapilli volcanic breccia with poorly selected lithic–pumiceous fragments. It contains RPB lithoclasts included in a vitreous quartz–feldspar re-crystallized glassy texture

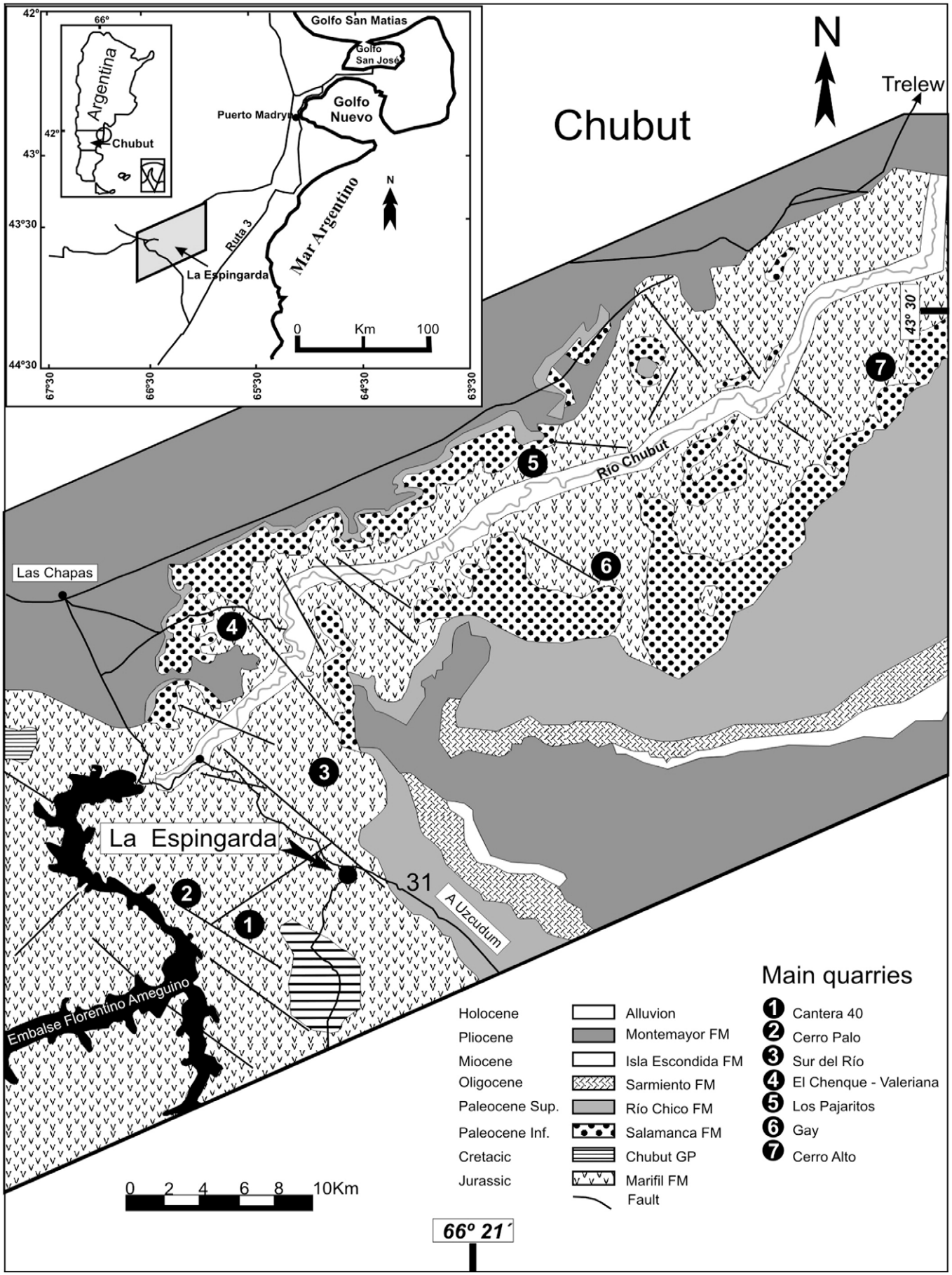

Fig. 1. Location and regional geology of La Espingarda and other major kaolin quarries at Valle Inferior del Rio Chubut (modified from Sacomani and Panza, 1998).

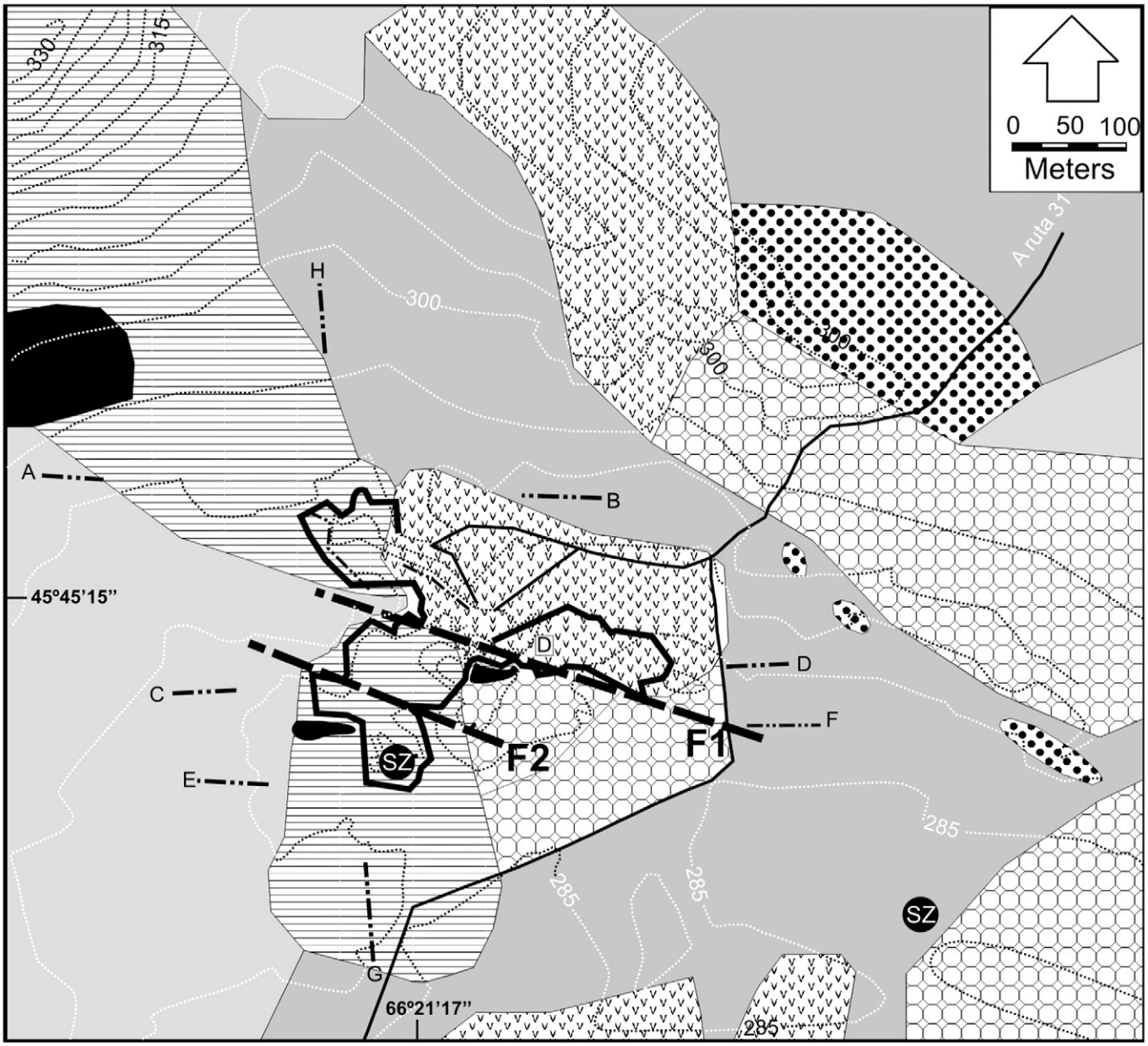

Fig. 2. La Espingarda deposit geology showing surface lithology and geological cross section locations.

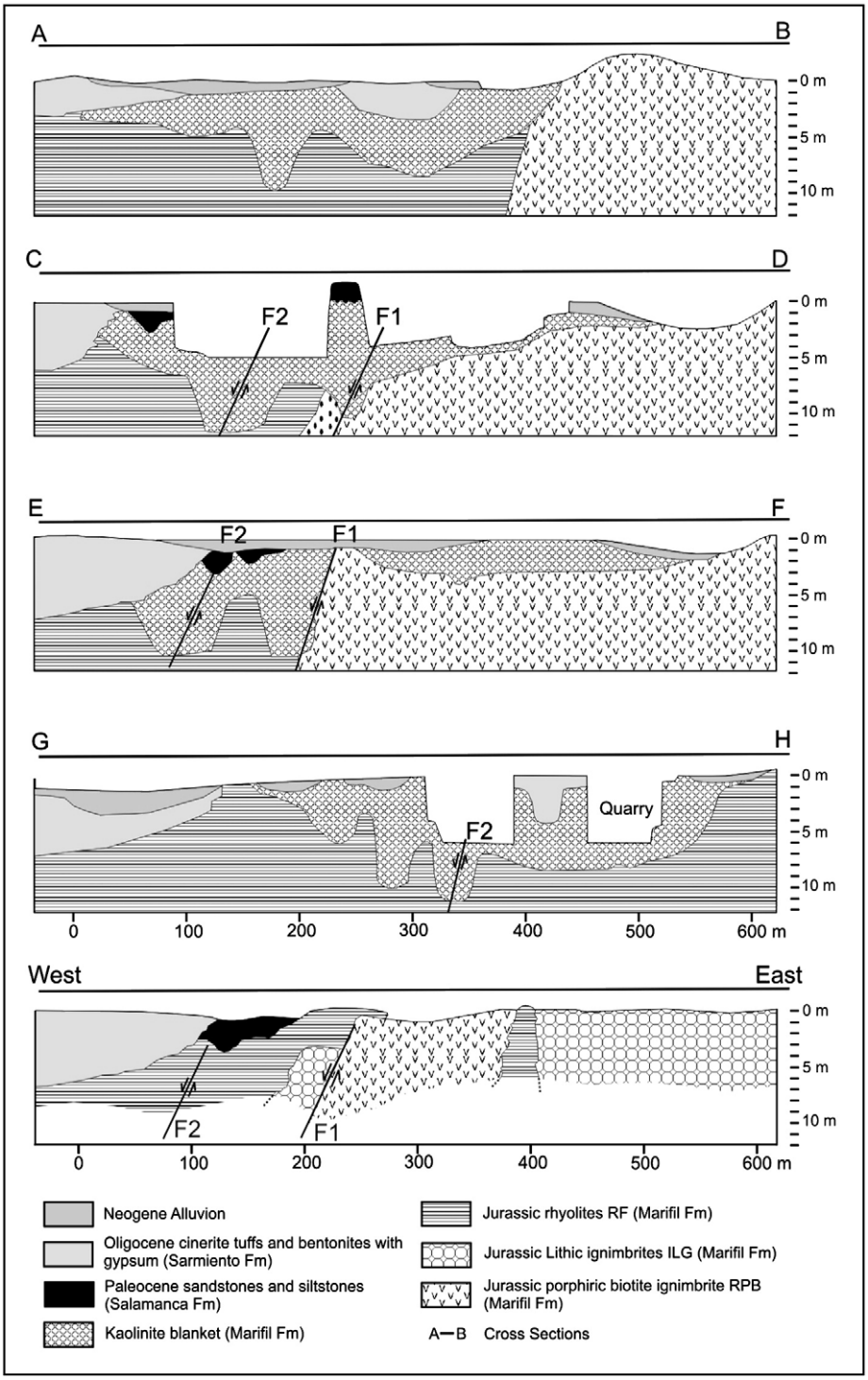

Fig. 3. Geological cross sections showing lateral and vertical alteration distributions (A–B, C–D, E–F, and G–H) and fresh rocks lithological relations (West–East). References in Fig. 2.

groundmass. Pumicites, quartz, feldspar fragments, and subordinate accessory minerals are also observed under the microscope. This rock is a non-welded ignimbrite with apparent porphyric texture (Fig. 4).

RF is a greyish purple-red rhyolite with lighter tones when weathered. Flow lines are mostly vertical but tend to be parallel when in contact with other vulcanites. In a working front, flow lines indicate their spill on a surface worked out on the RPB. This rhyolite has minor amounts of quartz and feldspars immersed in a re-crystallized fluidal aphanitic groundmass. Flow bands with some ghosts of orbicular textures are composed of quartz, fibrous feldspars and, in some cases, iron oxides (Fig. 4).

FT consists of green-yellowish, sub-horizontal, roughly stratified tuffs.

Stratigraphic relations among volcanic units are well observed on the outcrops. RPB has a fault contact with ILG. The fault is normal with ILG at the South as a descended block. Lithic fragments of RPB inside ILG allow us to conclude that RPB is older. RF intrudes into ILG and RPB along the fault plane and floods over RPB. FT lays over RPB and ILG (Figs. 2 and 3).

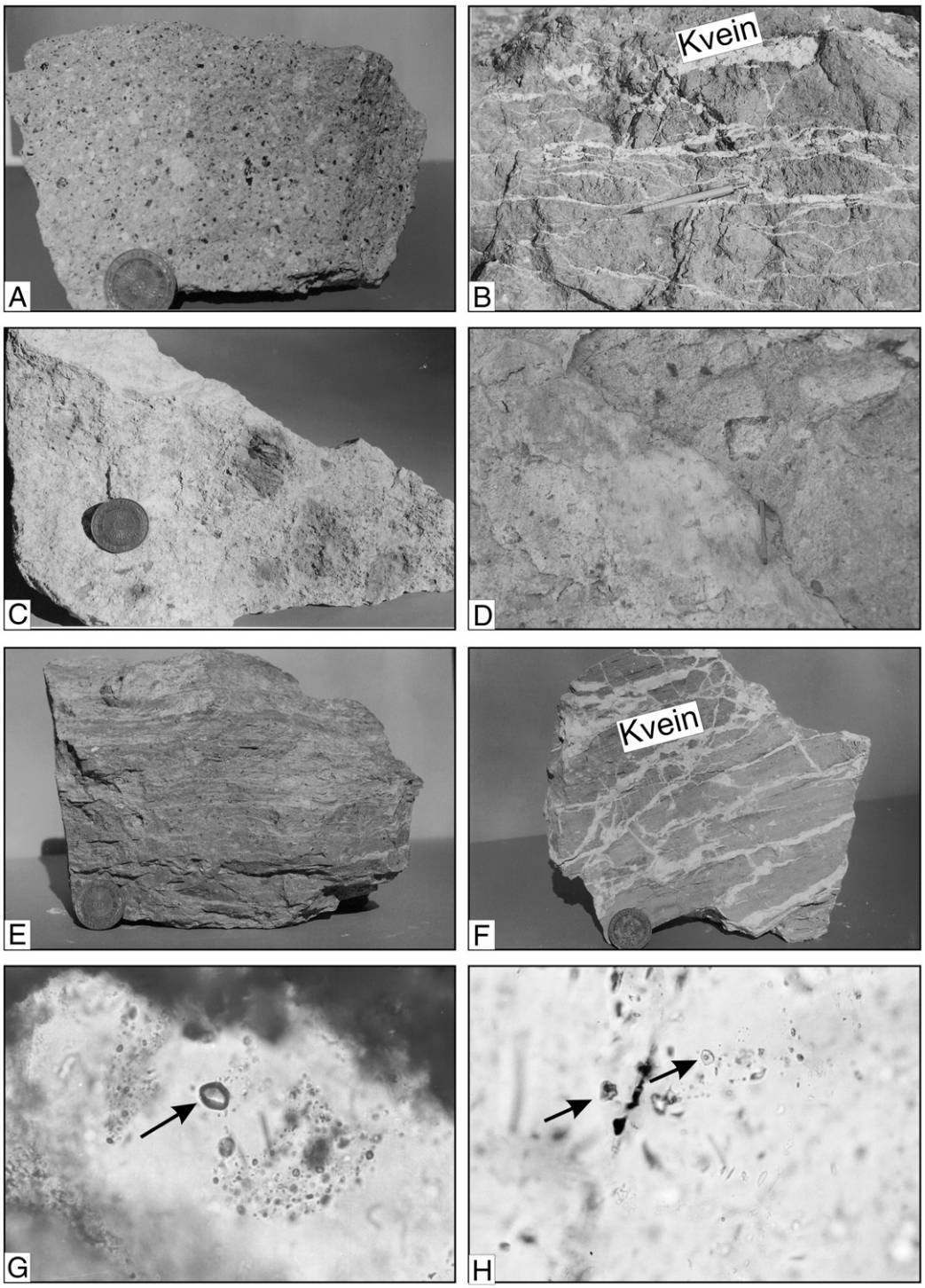

Fig. 4. Fresh and altered hand samples of RPB, ILG, RF and fluid inclusions. A — RPB unaltered sample showing lithoclasts, quartz fragments, irregular feldspar crystaloclasts, and scarce biotite. B — RPB: completely kaolinized rock cut by pure kaolinite veins. C — ILG breccia textures showing and pumicite fragments. D — completely and pervasively altered ILG. E — RF with fluidal textures showing bands with some quartz and feldspar phenocrystals in a vitreous groundmass. F — completely kaolinized RF showing kaolinite veins textures. G — quartz monophasic fluid inclusion. H — biphasic fluid inclusion.

5. Kaolinite blanket

5.1. Form

A pervasive kaolinization is observed in RPB, ILG and RF rock types, while pure kaolinite veins are seen mostly in RF outcrops. The TF is only slightly altered and its outcrops are some distance away from the quarry.

The kaolinite area has an ellipsoidal form, the longer axis being about 600 m long, roughly coinciding with one fault trace, and the shorter one being about 400 m long, covering a 20,000 m^2 area. The maximum kaolinization depth is close to 12 m along both sides of the fault. In the field the clay alteration exhibits a clear vertical zonation with a short passage between a fresh hard and compact rock to a soft earthly kaolin rock without substantial texture changes. There is no

clay zonation related to the fault trace. The alteration and its thickness are shown in Figs. 2 and 3.

5.2. Petrography

ILG presents a pseudoporphyric texture with reddish, greenish, and white lithoclasts in a pinkish rock to a bleached, soft, and earthy groundmass. Plagioclase laths in the groundmass are completely replaced by kaolinite. Tiny veins of pure kaolinite fill the rock joints. Some lithoclasts showed pumice residual textures pseudomorphically replaced by kaolinite and quartz. Re-crystallization quartz nets are also seen. The quartz crystalloclasts do not show any reaction rims, but small hematite crystals are seen following the flow lines. Altered RPB preserves the fresh rock texture and its alteration degree can be foreseen by the degree of rock cohesion. Biotite, plagioclase, and K-feldspar crystalloclasts are replaced by kaolinite and the pinkish groundmass is earthy and clay-rich (Fig. 4). Fine kaolinite veins with a stockwork texture were seen in restricted places. RF presents thin flow bands which are alternating dark- and light-coloured. Biotite crystals are replaced by kaolinite. This rhyolite has a very fine groundmass consisting of kaolinite and quartz. Abundant pure kaolinite veins with a stockwork texture cut the reddish altered rhyolite.

In one restricted sector scarce fine quartz veins with crystals growing from the walls cuts the RF flow lines. These veins cuts fully kaolinite replaced lithoclasts and have kaolinite-filled vugs. These veins were also found cutting a slightly altered rhyolite at the quarry bottom. A small massive quartz outcrop (<2 m^2) is related to the fault. There is no clay zonation related to any quartz manifestation.

Careful observations show that there are at least three kaolinite generations. The pervasively kaolinized rocks (K1) with fully altered lithoclasts are cut by quartz veins with kaolinite (K2) filling the vugs. The pure kaolinite veins (K3) that cut the pervasively altered rhyolite have never been observed crossed by any quartz vein (Fig. 5).

5.3. X-ray, SEM, and TEM clay mineralogy

The kaolin mineralogical composition is simple and regular. Whole X-ray bulk rock sample powder diagrams from the three altered lithofacies show quartz, K-feldspars, plagioclase, kaolinite, and illite with different reflection intensities according with its alteration degree. The illite presence was confirmed on oriented natural, glycolated and heated X-ray <2 μm fraction.

The X-ray quantitative mineralogical composition of typical fresh, medium and highly altered rocks is shown in Table 1. The quartz remained practically constant in all the alteration stages, but biotite, plagioclase and in the last term sanidine are replaced by kaolinite. The maximum kaolin content is about 40/57% in the whole highly altered rock and reaches 98% in the washed samples <2 μm fraction.

Mineralogical composition changes with the degree of alteration and the different lithology. During alteration, plagioclase and biotite are transformed into kaolinite; illites (Srodon and Eberl, 1987) are

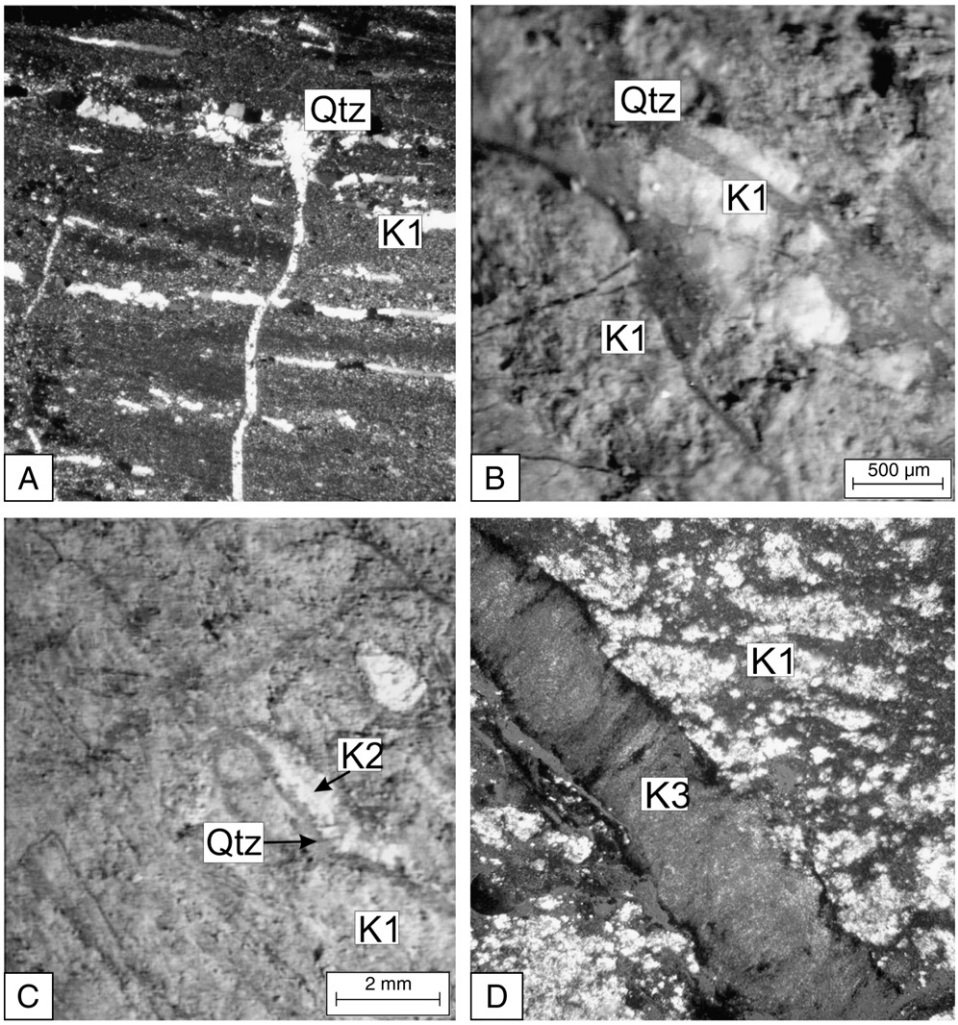

Fig. 5. Kaolinite generations. A — kaolinite 1 (FR pervasively kaolinized rock cut by a very fine quartz vein) B — kaolinite 1 (altered lithoclast cut by quartz veinlets). C — kaolinite 2 (PBI kaolinized rock cut by quartz veins with kaolinite growing at the vugs walls). D — kaolinite 3 (kaolinite veins cutting the former arrangements). Qtz: quartz; K: kaolinite.

Table 1
X-ray quantitative mineralogy (wt.%).

Lithofacies	Intensity	Ka	Il	Q	Fd	Bi	Acc	Hi	Si
ILG	Fresh			28	68	4			
	Medium	35	6	51	4				
	High	28		53	1		3		
	Washed	68*	3	26			3	0.76	0.87
PBI	Fresh			53	42	5			
	Medium	34	13	30	23				
	High	31**		44	21		4		
	Washed	84**		12			4	0.56	0.94
RF	Fresh			50	50				
	Medium	20	3	48	29				
	High	35***		52	7		6		
	Washed	70***		21			9	0.32	1.21
Vein		100						0.82	0.79

References: ILG: lithic ignimbrite, PBI: rhyolitic porphyric biotite, RF: fluidal rhyolite, Veins: venillas. Intensity: alteration degree. Hi and Si: Hinckley (1963) and Stoch's (1974) indices of kaolinite structural order. *Low, ** Medium, ***High halloysite semi quantitative abundance. Ka: kaolinite, Il: illite, Q: quartz, Fd: feldspar, Bi: biotite, Acc: accessories.

present only in the intermediate alteration stage in all lithofacies. Among feldspars, sanidine is more resistant than plagioclase, because it persists until the most advanced alteration stages. Quartz remained practically constant in the alteration stages, while kaolinite replaced feldspars progressively; thus, the more intensely altered rocks consist almost exclusively of quartz and kaolinite (Table 1).

A moderately disordered kaolinite is seen in the X-ray powder diagrams of ILG and RPB and in the RF the halloysite's presence is suspected (Fig. 6). The Hinckley crystallinity index (Hinckley, 1963) of the kaolinites is 0.87 for ILG, 0.82 for veins, 0.56 for RPB, and 0.32 for RF. These values correspond to moderately disordered kaolinites. The Stoch index (Stoch, 1974) values obtained are 0.79 for veins, 0.87 for ILG, 0.94 for RPB and 1.21 for RF, so they fall between disordered (> 1.0) and ordered (<0.7) kaolinites. Therefore, the structural order of kaolinite is ILG = veins > RPB > RF.

The SEM images of RPB show an open texture with short and irregular kaolin books, corroded feldspars and on TEM some illite fibers are seen (Fig. 6). To reinforce the open texture rock density is given. Fresh rock density is 2.40 g/cm^3 and 1.98 when altered. At ILG shorts and open kaolin books with scarce halloysite fibers are seen. Fresh rock density is 2.24 g/cm^3 and 1.54 when altered. At RF almost exclusively halloysite fibers dispensed over minor hexagonal kaolinite platelets are seen (Fig. 6). Fresh rock density is 2.45 g/cm^3 and 1.65 g/cm^3 when altered. The SEM pictures are in agreement with kaolinite structural order found using X-ray diagrams. Vein kaolinite crystals are small and with less defined ledges. Its aggregates resemble some botroidal textures (Fig. 6).

Alteration had a diverse effect on the three lithofacies, causing differential paragenesis (Table 1, Fig. 6):

- The coarse-grained lithic ignimbrite (ILG) is composed of quartz and kaolinite with minor halloysite.
- The biotite porphyric ignimbrite contains quartz and sanidine along with similar amounts of kaolinite and halloysite.
- The rhyolite flow (RF) consists of quartz and halloysite with minor kaolinite and sanidine.

5.4. Kaolinite isotopes

Previous data on pure kaolinite veins showed values of 18.3 δ^{18}O‰ and −59.0 δD‰ (Cravero et al., 1991). Two new samples showed values of 19.3 and 19.1 δ^{18}O‰; −83.0 and −82.0 δD‰. The ILG kaolinite values of 13.0 δ^{18}O‰ and −85.0 δD‰ differ slightly from the previous values and plots slightly removed from the water line. For the ILG kaolinite values interpretation, the equation of Sheppard and Gielg (1996) was used considering that currently isotopic values for surface water in Santa Cruz are −6.6 δ^{18}O‰ and −51 δD‰ while for average Jurassic water are of 6.93 ± 1.55 δ^{18}O‰ and −42.19 ± 12.32 δD‰ (Cravero et al., 1991).

6. Quartz fluid inclusions

The quartz veinlets cutting the argillized groundmass are 2 to 40 μm thick. The quartz has crystals growing upward from the walls with pyramidal terminations. In one vein, a small hematite–ilmenite crystal was found. Limited and small fluid inclusions were found in quartz growth zones. They are isolated, primary, and correspond to two types. One type has only one phase (L) and the other has two phases (L–V) with a small vapour bubble (<10%) at room temperature (Fig. 4). In two-phase inclusions, homogenization temperatures range from 144 to 277 °C (19 measurements) with a higher frequency between 150 and 180 °C (14 measurements). In one sample, freezing assays indicate the appearance of a eutectic point at −21 °C with a final melting point of −0.2 °C, corresponding to a low salinity fluid (equivalent to <1% mass NaCl).

7. Geochemistry

7.1. Unaltered rocks

The fresh rocks according to TAS diagrams (Lemaitre, 1989) are rhyolites with silica between 74 and 77% and alkalis between 7.9 and 9.7% (Table 2). K_2O concentrations are higher than those of Na_2O, attributing these rhyolites to the sub-alkaline series (Irvine and Baragar, 1971). These rocks were formed by peraluminous magma (Shand, 1927; Maniar and Piccoli, 1989) coming from extensional areas with cortical anatexis (Uliana et al., 1985).

7.2. Altered rocks

In the argillized rocks two different alteration paths can be observed: one leading to an extensive kaolinization, observed in all lithotypes. The other one produced silicification superimposed on kaolinization. The distribution of major and minor elements in fresh and altered rocks shows that significantly different chemical trends occurred both in the two alteration paths and in the three lithotypes (Table 2).

In a framework common to the whole deposit, a different geochemical behaviour was found for an increasing alteration degree, as outlined by a multivariate statistical analysis (Fig. 7):

- Alkalis and alkaline-earth elements were leached decreasing their concentration in all lithotypes (Na, K, and Rb) but RF (Mg, Ca, Sr, and Ba).
- Al, Sc, Ti, Ta, and Th behave as immobile elements, being progressively enriched in all lithotypes, as do Be, Zr, Y, Hf, and HREE (but in RF) as well as P and LREE (but in ILG).
- Only in the kaolinization path, a weak increase of hydrothermal-related elements, such as S, Mo, Cd, Sb, W, and U, occurred.
- Transition elements, such as V, Cr, Mn, Fe, Co, Ni, Cu, and Zn (and also As, Cs, and Pb), show variable trends depending on the alteration path and the lithotypes, so that no general pattern is evident.
- Trace elements such as Se, Br, Nb, Ag, Ir, Au, Hg, and Bi do not vary significantly.

Interestingly enough, the alteration of the rhyolite flow (RF), that gave rise to abundant halloysite, involved, on the one hand, the leaching of elements thought to be nearly immobile — such as Be, Zr, Y, Hf, and HREE — and, on the other hand, the stabilization of alkaline-earth elements.

On the other hand, the alteration path involving kaolinization + silicification produced, together with an obvious change in the

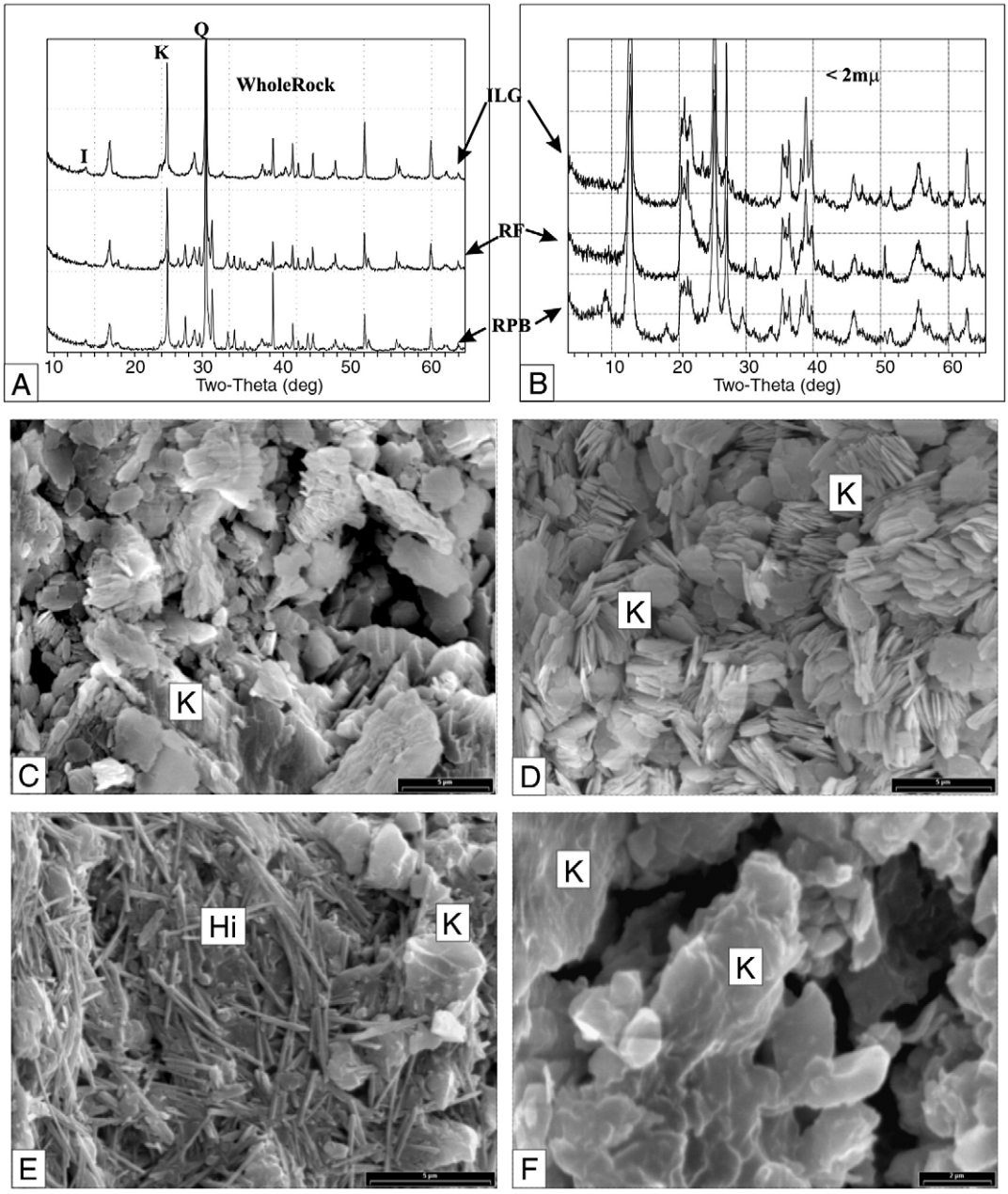

Fig. 6. A and B — ILG, RF, and RPB typical whole rock and <2 μm X-ray diagrams. C — RPB SEM open texture with short kaolinite books, scarce short illite fibers, and corroded feldspars. D — ILG SEM open texture with short and open kaolinite books and scarce halloysite fibers. E — RF SEM showing halloysite fibers disposed over kaolinite plates. F — SEM kaolinite from pure veins showing small and not well formed kaolin crystals.

alumina/silica ratio, the immobilization of Co and Ni as well as the mobilization of Be, Mn, Fe, Zn, Zr, Hf, Pb, Th, and U.

This general picture is confirmed by a classical gain and loss approach of Hildreth diagrams (Hildreth, 1981) (Fig. 8). In particular, it is clearly seen in ILG that the main gains are Al, Ti, and LoI, and the main losses correspond to Na, Ca, K, and P. In the case of PBI in an advanced alteration degree, gains of Ti, P, and H_2O as well as losses of Na, Ca, K, Mg, Fe, and Mn are recorded. As alteration went on RF, Ti, P, and LoI were gained, while Na, Ca, K, Mn, and Fe were lost. With Hildreth's diagrams, an important loss of Na and K as well as remarkable water enrichment is observed in all rocks. The main changes concern: losses of Ca, Fe, and Mn, gains of Ti, and variable behaviour of Al, Si, and Mg. RPB and ILG have Ni enrichment and Cu, Sr, and Ba impoverishment in common. RF shows a loss in Zr, but gains in Ba, La, and Ce (Fig. 8). SO_3 versus P_2O_5 correlation shows a little increase in S and P contents in the altered rocks.

8. Discussion

La Espingarda, and many residual kaolin deposits along the Chubut river valley are found in lowlands along the Jurassic rhyolite paleosurface and are covered by sedimentary rocks that include secondary *ball clay*-type deposits.

A warm and humid climate with rainy periods where kaolinite can be formed (Murray and Keller, 1993; Velde, 1999) for Jurassic to Palaeocene times is supported by the paleontological record (Volkheimer, 1967; Archangelsky, 1967; Musacchio and Chebli, 1975; Pothe de Baldis, 1976).

The tabular shape of the kaolinite body with its lateral extension much larger than its thickness (ratio >60/1), excludes a hypogene hydrothermal origin because this latter would generate alteration zones with more vertical than lateral extensions around the conduits (Stoffegren, 1985; Hayba et al., 1985; White, 1991; Heinrich et al., 1999). The deposit shape could be compatible with a kaolinization

Table 2
Whole rock chemical composition of fresh, medium and highly and altered rocks.

Facies		ILG				PBI				RFI				
Alteration		Fresh	Interm	High	High	Fresh	Interm	High	High	Fresh	Fresh	Interm	High	High
Sample		1	2	3	4	5	6	7	8	9	10	11	12	13
SiO_2	%	74.25	75.41	73.67	74.71	76.05	75.56	82.98	72.31	77.18	74.83	75.64	84.70	73.56
TiO_2	%	0.18	0.20	0.21	0.23	0.15	0.17	0.17	0.22	0.11	0.14	0.19	0.19	0.22
Al_2O_3	%	13.16	14.95	15.77	15.51	12.09	13.52	11.61	16.22	11.15	13.82	13.87	10.23	15.92
Fe_2O_3	%	1.61	1.17	1.31	1.34	1.16	1.21	0.41	1.51	1.21	1.32	1.17	0.31	1.46
MnO	%	0.03	0.03	0.03	0.04	0.03	0.03	0.01	0.03	0.07	0.06	0.02	0.02	0.02
MgO	%	0.19	0.17	0.24	0.17	0.13	0.07	0.02	0.04	0.04	0.05	0.05	0.01	0.06
CaO	%	0.21	0.12	0.20	0.12	0.22	0.07	0.07	0.05	0.10	0.10	0.08	0.05	0.14
Na_2O	%	3.80	0.13	0.32	0.13	2.79	0.42	0.14	0.73	2.50	4.78	0.15	0.15	0.58
K_2O	%	4.58	1.41	1.36	1.09	5.55	5.05	0.03	2.54	5.44	4.94	4.75	0.19	0.29
P_2O_5	%	0.04	0.02	0.03	0.02	0.02	0.02	0.03	0.03	0.02	0.01	0.02	0.04	0.02
C	%	n.d.	n.d.	n.d.	0.04	n.d.	n.d.	n.d.	0.02	n.d.	n.d.	n.d.	n.d.	0.05
L.o.I.	%	0.97	4.97	7.18	5.98	0.57	2.73	4.91	5.89	0.70	0.34	3.29	4.15	7.40
Total	%	99.02	98.58	100.32	99.38	98.76	98.85	100.38	99.59	98.52	100.39	99.23	100.04	99.72
Ag	ppm	<0.3	<0.3	0.9	1.0	<0.3	<0.3	<0.3	<0.3	0.8	1.2	<0.3	0.7	0.5
As	ppm	14	3	3	3	3	5	2	9	6	4	4	7	10
Au	ppb	<5	<5	<5	<2	<5	<5	41	<2	<5	<5	<5	<5	<2
Ba	ppm	1188	31	166	70	425	329	77	168	17	11	106	36	23
Be	ppm	2	3	4	4	2	2	2	3	3	3	1	1	2
Bi	ppm	<2	<2	<2	<2	<2	<2	<2	<2	<2	<2	<2	<2	<2
Br	ppm	<1	<1	<1	<0.5	<1	<1	<1	<0.5	<1	<1	<1	<1	0.8
Cd	ppm	<0.3	<0.3	<0.3	0.7	<0.3	<0.3	<0.3	0.4	<0.3	<0.3	<0.3	<0.3	0.6
Co	ppm	3.0	1.0	3.0	1.2	2.0	1.0	2.0	1.1	1.0	2.0	1.0	2.0	0.9
Cr	ppm	<2	<2	2	6	53	6	33	3	35	28	2	27	3
Cs	ppm	7.3	8.9	13.2	5.9	3.2	3.6	1.9	1.8	2.5	1.7	4.9	3.7	1.6
Cu	ppm	6	8	2	5	3	4	3	6	5	4	3	3	4
Hf	ppm	4.2	4.1	7.3	6.5	3.5	2.7	3.7	5.1	7.3	7.9	4.6	5.9	6.2
Hg	ppm	n.d.	n.d.	n.d.	<1	n.d.	n.d.	n.d.	<1	n.d.	n.d.	n.d.	n.d.	<1
Ir	ppb	<5	<5	<5	<2	<5	<5	<5	<2	<5	<5	<5	<5	<2
Mo	ppm	<5	<5	<5	3	<5	<5	<5	2	<5	<5	<5	<5	4
Nb	ppm	n.d.	n.d.	20	n.d.	n.d.	n.d.	12	n.d.	n.d.	n.d.	n.d.	18	n.d.
Ni	ppm	4	1	<1	4	5	3	20	3	4	<1	<1	18	3
Pb	ppm	19	9	25	20	24	15	18	23	22	32	36	21	33
Rb	ppm	129	114	128	133	200	158	<20	94	200	201	204	<20	18
S	ppm	20	200	150	180	30	100	90	430	20	20	160	140	440
Sb	ppm	0.3	0.3	1	0.6	0.5	0.4	0.6	0.8	0.4	0.3	0.8	0.9	0.7
Sc	ppm	2.8	4.0	6.2	5.2	2.1	3.7	2.4	4.5	2.6	2.2	2.9	3.1	4.8
Se	ppm	<3	<3	<0.3	<0.5	<3	<3	<3	<0.5	<3	<3	<3	<0.3	<0.5
Sr	ppm	97	10	22	11	42	15	7	9	10	13	12	7	11
Ta	ppm	<1	1.0	2.0	1.8	<1	1.0	2.0	1.7	<1	<1	2.0	2.0	1.8
Th	ppm	15.9	24.9	29.3	31.0	15.3	16.3	15.7	24.4	22.3	25.4	22.5	19.9	30.0
U	ppm	2.1	2.5	3.3	4.2	2.2	1.1	0.9	3.7	2.7	2.2	2.3	1.8	4.3
V	ppm	50	26	19	11	7	24	6	34	<5	5	22	12	46
W	ppm	<0.3	<0.3	<0.3	1	<0.3	<0.3	<0.3	4	<0.3	<0.3	<0.3	<0.3	3
Zn	ppm	30	44	38	50	28	30	12	32	62	53	37	27	23
Zr	ppm	147	211	276	262	105	134	135	160	199	226	189	164	170
La	ppm	168	44	55	46	41	44	24	67	30	34	67	50	73
Ce	ppm	236	69	79	78	100	102	35	96	51	64	110	60	123
Nd	ppm	95	28	26	35	22	26	13	47	18	20	30	21	55
Sm	ppm	19.1	4.6	5.5	5.2	4.6	5.4	2.3	7.8	6.0	6.9	6.2	4.1	8.4
Eu	ppm	2.9	0.5	0.6	0.6	0.6	0.7	0.2	1.0	<0.1	0.3	0.8	0.5	0.9
Tb	ppm	1.2	<0.5	<0.5	0.8	<0.5	<0.5	<0.5	0.9	0.9	1.4	0.8	<5	1.3
Y	ppm	25	24	37	25	19	24	10	20	43	49	28	23	24
Yb	ppm	4.0	3.1	4.5	3.9	2.4	2.8	1.3	3.1	5.7	4.1	3.1	2.3	3.6
Lu	ppm	0.60	0.46	0.70	0.59	0.36	0.42	0.20	0.45	0.84	0.61	0.46	0.33	0.54

caused by the action of magmatic vapour condensates in phreatic zones. In this case the kaolinite formation temperatures rarely exceed 200 °C (Schoen et al., 1974; Hayba et al., 1985). The tabular form is also compatible with weathering.

The mineralogical composition of the three lithofacies changes with the alteration degree. Kaolinite, with subordinate illite, replaced plagioclase, biotite, and sanidine so that in completely altered rocks only kaolinite and quartz are present. The mineralogy presents a clear vertical zonation. The mineralogical composition, without dickite, pyrophyllite, sulphides or alunite is an argument against a hydrothermal origin (Sillitoe, 1993; Simeone et al., 2005). The gibbsite absence could be explained considering an incompletely developed paleo-weathered profile (Thiry et al., 1999).

The degree of structural order of kaolinite (i.e. Hinckley or Stoch's indices) is of limited genetic significance. Under SEM, PBI, ILG, and RF kaolins show an open texture, expanded kaolinite books, high porosity, and low bulk density, similar to those described for samples from weathering environments (Keller, 1976). The kaolinite structural order surely depends on protolith type, grain seize and fluid circulation. The higher values are at the coarse ILG and on kaolinite veins. The halloysite seems to be later than kaolinite plates and its abundance linked to major fluids circulation at the RF that contains mostly of the kaolinite veins.

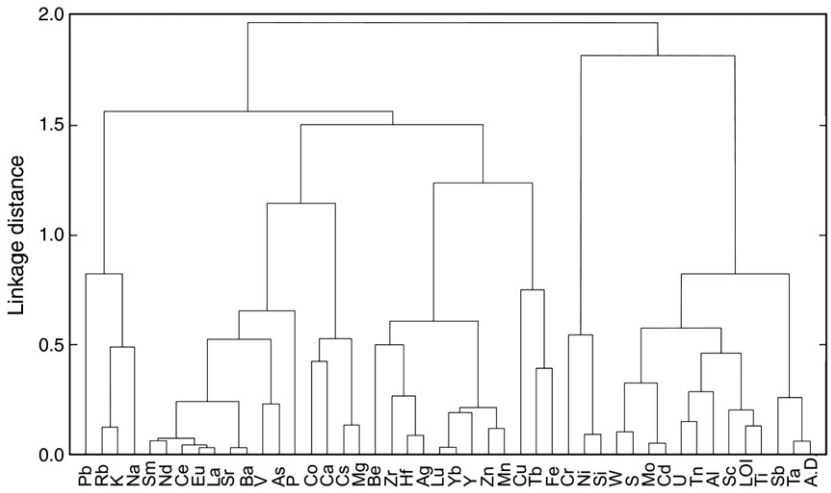

Fig. 7. Cluster analysis (linkage method: complete linkage; distance measurement: Pearson's $1-r$) showing the geochemical affinity of major and minor elements during the alteration process. A.D. = alteration degree.

Previous kaolinite isotope values in the area were interpreted as due to weathering (Cravero et al., 1991; Domínguez and Cravero, 1999). Two new determinations on pure kaolinite veins plotting along the kaolinite line confirm the weathering origin. The ILG isotopic values of 13.0‰ $\delta^{18}O$ and −85.0‰ δD could be explained by either a temperature increase to near 60 °C in the surface waters (using the Sheppard and Gielg's equations, 1996) or a small contribution of magmatic vapours (Sakai and Matsubaya, 1977).

The presence of quartz veins with fluid inclusions with homogenization near room to 150–180 °C temperatures and with low salinity (equivalent to <1% mass NaCl), is a strong argument to support a hot water participation in the kaolinite formation. Pure

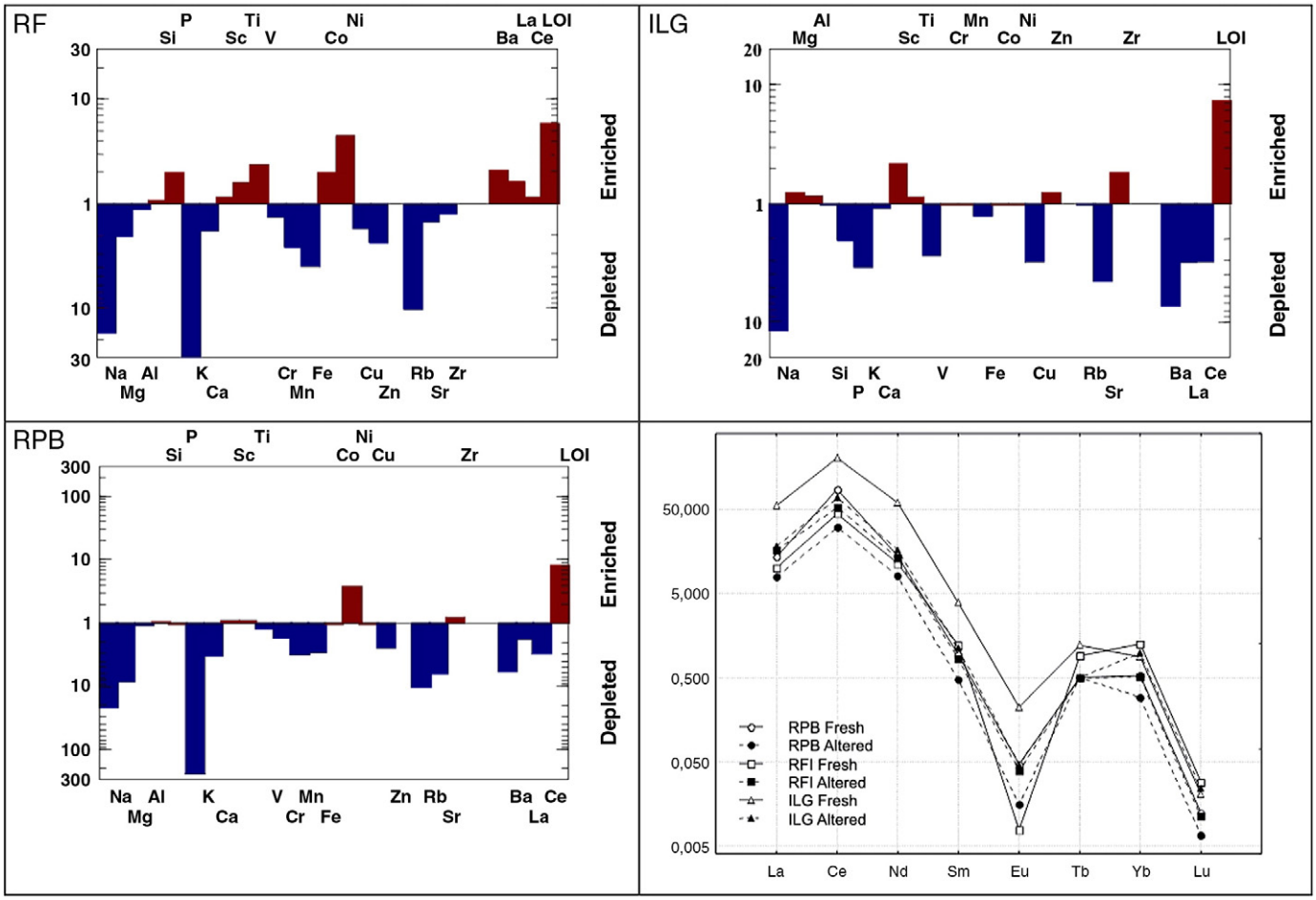

Fig. 8. Hildreth's (1981) diagrams showing gains and losses of major and minor elements in the three lithofacies: fluidal rhyolite A: ILG, B: RPB and C: RF; D: distribution pattern of Rare Earth Elements, normalized to chondrites (Nakamura, 1974).

water inclusions have been found in samples from low pressure, near surface, hot spring environments (Roedder, 1977). Also the quartz crystals inherited chalcedonic textures typical of an initial silica gel of hydrothermal precipitation (Dong et al., 1995). In a shallow epithermal system the isotopic values of kaolinite lie close to the kaolinite line, which point to the clay formation during weathering or supergene processes consistent with a steam-heated water of 25–50 °C (Simeone et al., 2005).

Geochemical gain and loss balances show that the alteration trend is similar to that of granite weathering in laboratory simulations (Schmidt, 1999). These results coincide with those shown in CIA diagrams for weathered granites (Nesbitt and Young, 1989). In Hildreth's diagrams, the three lithofacies have in common the following: Ni enrichment and Cu, Sr, and Ba depletions as in weathered profiles. Also the altered rocks have S and P contents slightly higher than equivalent fresh rocks and this could be attributed to a hydrothermal influence. However, Au, Ag, As, Sb, Hg, Ba, Mo, Pb, S, Sr, and Ta contents, usually taken as mineralization pathfinders in hydrothermal hot spring systems, are lower than those found even in sterile gold deposits (Nelson, 1988 — Table 3). The Cu, Au, As, and B low values point to a limited magmatic contribution because these elements are rich in high temperature magmatic vapours (Heinrich et al., 1999).

REE distribution pattern, normalized to chondrite (Nakamura, 1974), is similar in the three unaltered lithofacies, presenting a higher concentration of LREE with respect to HREE and marked anomalies of Ce (positive) and Eu (negative). REE behaviour during the alteration is not uniform in the three lithotypes, though the general pattern resembles that of unaltered rocks (Fig. 8D). It seems that Rare Earths behave as immobile elements only in PBI, where the alteration degree in not very intense, as just a partial transformation of feldspars occurred. The strong kaolinization of ILG involved the mobilization of LREE, while the halloysitization of RF implied the partial leaching of HREE. The differences in mineralogy and Be, Zr, Y, Hf, HREE and alkaline-earth elements in the RF are attributed to its highest meteoric water leaching rate evidenced by the abundance of kaolinite veins.

According to kaolinite paragenesis and geological facts a reasonable interpretation for the genesis of this deposit is that the weathering conditions that formed the kaolinite blanket started before and then persisted after the overprint of parasitic short lived hot spring hydrothermal system. The late veins of pure kaolinite were formed by meteoric waters.

Hydrothermal kaolinite mines are located around and beneath silicified, erosion-resistant hills; they have a clear clay lateral zonation that includes some of the following minerals: dickite, alunite, pyrophyllite, or pyrite interpreted as belonging to a high sulphide mineralization system (Ducart et al., 2006). Isotopic δ^{18}O‰ and δD‰ kaolinite contents are removed from the supergenic/hypogenic line. The anomalous contents of As, S, Ba, and Ag are compatible with a weak mineralization range (Marfil et al., 2005). Epithermal low sulfidization precious metal mineralization is strongly associated to erosion-resistant fracture-related silicification with subtle or no kaolinite alteration and several high grade bonanza ore shoots are blinds.

Table 3
Geochemical pathfinders for hot spring epithermal deposits (Nelson, 1988).

	Reference values		La Espingarda kaolins		
ppm	Known deposits	Barren deposits	ILG	PBI	RF
Ag	15.2	6.5	1.0	<0.3	0.5
As	183	162	3	9	10
Au	1.9	0.7	<.002	<.005	<.002
Ba	889	557	70	168	23
Hg	36	22	<1	<1	<1
Sb	215	21	1.0	0.8	0.7
Ta	12	2	1.8	1.7	1.8

La Espingarda has lower geochemical values than that registered for barren hot spring deposits.

9. Conclusions

Very likely, the genesis of the deposit is that weathering forming the kaolinite blanket started before and persisted after the overprint of a steam heated hot water action. The late veins of pure kaolinite were formed by meteoric waters.

This deposit and numerous similar ones in the surrounding area are located on a topographic depression associated with rhyolitic flows and ignimbrites of Jurassic age.

Three volcanic rhyolitic rocks types were kaolinized and three kaolinite generations were identified. The first kaolinite generation is pervasive widespread and affects all the rocks. The second one is rare and appears as vuggy fillings in the quartz veins that cross cut kaolinized rocks; and the third one appears as abundant small white veins in the fluidal rhyolite.

The mineralogical composition is simple with a downward zonation (i.e. kaolinite ± halloysite → kaolinite + illite → unaltered rock). Each lithotype has its proper mineralogical arrangement promoting characteristic ceramic behaviour.

The Au, Ag, As, Sb, Hg, Ba, Mo, Pb, S, Sr, and Ta contents are lower than those found in sterile hydrothermal hot spring gold systems. Neither the kaolinite genesis nor the trace element contents and the drill data support the existence of any precious metal mineral deposit beneath the kaolinite blanket bottom. Alteration areas with these characteristics do not have any metallic exploration potential.

In Patagonia hydrothermal kaolinites are located around and beneath silicified, erosion-resistant hills. They have a clear clay lateral fault related zonation that includes some of the following minerals: dickite, alunite, pyrophyllite, or pyrite. The isotopic δ^{18}O‰ and δD‰ in kaolinite are compatible with hydrothermal high temperature fluids and As, S, Ba, and Ag contents are within the range of weak geochemical anomalies.

Acknowledgements

This work is part of the Doctorate research work of C Iglesias at the Universidad Nacional del Sur and includes activities carried out within the framework of the CNR-CONICET 2003–2004 bilateral agreement. Authors are grateful to UNS, CNR, CONICET and Piedra Grande for their financial support. Many thanks to M. Garrido, R. Salomón, and G. Arzadún for the help during the draft reviewing. Many thanks to E. Galan, G. Lagaly and anonymous reviewers for their comments.

References

Angelelli, V., Stegman, E., 1948. Estudio sobre arcillas y caolines de la Republica Argentina, yacimientos Blaya Dougnac, Linares, Villanueva y Hércules. Revista Industria Minera Buenos Aires, pp. 47–54.

Aparicio, P., Galán, E., 1999. Mineralogical interference on kaolinite crystallinity index measurements. Clays and Clay Minerals 47 (1), 12–27.

Archangelsky, S., 1967. Estudio de la Formación Baquero, Cretácico inferior de Santa Cruz, Argentina. Revista del Museo de La Plata, Paleontologia 5, 63–171.

Bertels, A., 1973. Bioestratigrafía del cerro Bororó, provincia del Chubut. Actas 5º Congreso Geológico Argentino. T III.

Bethke, P.M., 1984. Controls on base and precious mineralization in deep epithermal environments: U.S. Geological Survey, Open File Report, vol. 84-890. 40 pp.

Bodnar, R.J., 1992. The system H_2O–NaCl. PACROF I IV, Program and abstracts, pp. 108–111.

Clayton, R.N., Mayeda, T., 1963. The use of bromine pentafluoride in the extraction of oxygen from oxides and silicates from isotopic analysis. Geochemistry and Cosmochemistry Acta 27, 47–52.

Cravero, M.F., Domínguez, E.A., Murray, H.H., 1991. Valores d18O y dD en caolinitas indicadores de un clima templado-húmedo para el Jurásico superior-Cretácico inferior de la Patagonia. Revista de la Asociación Geológica Argentina XLVI (1–2), 20–25.

Domínguez, E., Murray, H., 1995. Genesis of the Chubut River Valley Kaolin Deposits, Argentina, and Their Industrial Applications. In: Churchman, J., Fitzpatrick, R., Eggleton, R. (Eds.), Clays: Controlling the Environment. Proc. 10th International Clay Conference. Australia, 1993. CFIRO Publishing, Melboune, Australia, pp. 129–134.

Domínguez, E., Cravero, M.F., 1999. Los recursos de caolín de Chubut y Santa Cruz. In: Recursos minerales de la República Argentina Zappettini E.O. (Ed). Instituto de geología y recursos minerales. Secretaría de Estado de Geología y Minería de Argentina, Buenos Aires, Argentina. Anales 35, pp. 1265–1272.

Dong, G., Morrison, G., Jeireth, S., 1995. Quartz texturas in epithermal veins, Queensland. Clasification, origin and implications. Economic Geology 90, 1841–1856.
Ducart, D.F., Crósta, A.P., Souza Filho, C.R., Coniglio, J., 2006. Alteration mineralogy of the Cerro La Mina Epithermal Prospect, Patagonia, Argentina: field mapping, short-wave infrared spectroscopy, and Aster Images. Society of Economic Geologists 101, 981–996.
González Guillot, M., De Barrio, R., Gamem, F., 2004. Mina Martha, un yacimiento epitermal en el Macizo del Deseado, provincia de Santa Cruz. In: Brodtkob, M.K., Koukharsky, M., Quenardelle, S., Montenegro, T. (Eds.), Avances en Mineralogía, Metalogenesis y Petrología 2004. 7ª Congreso de Mineralogía y Metalogenia. Río Cuarto. Córdoba. Argentina, pp. 199–204.
Hayase, K., 1969. Génesis del yacimiento de caolín de la mina Villegas, Provincia del Chubut, Republica Argentina. Revista de la Asociación Geológica Argentina XXIV, 55–71.
Hayba, D., Bethke, P., Helad, P., Foley, N., 1985. Geologic, Mineralogic, and Geochemical Characteristics of Volcanic-hosted Epithermal Precious Metal Deposits. In: Berger, B.R., Bethke, P.M. (Eds.), Geology and Geochemistry of Epithermal Systems: Reviews in Economic Geology, vol. 2, pp. 129–167.
Hedenquist, J., Arribas, R., González-Urien, E., 2000. Exploration for Epithermal Gold Deposits. In: Hagemann, S., Brown, P.E. (Eds.), Gold in 2000: Reviews in Economic Geology, vol. 13, pp. 245–277.
Heinrich, C., Gunter, D., Audetat, A., Ulrich, T., Frinschkenecht, R., 1999. Metal fractionation between magmatic brine and vapor determined by microanalysis of fluid inclusions. Geology 27, 755–758.
Hildreth, W., 1981. Gradients in silica magma chambers: implications for lithospheric magmatism. Journal of Geophysics Research 86, B10153–B10192.
Hinckley, D., 1963. Variability in "crystallinity" values among the kaolin deposits of the Coastal Plain of Georgia South Carolina. Clay and Clay Minerals 11, 229–235.
Irvine, T., Baragar, W., 1971. A guide to the chemical classification of the common volcanic rocks. Canadian Journal of Earth Sciences 8, 523–548.
Keller, W., 1976. Scan Electron Micrographs of Kaolin Collected from Diverse Environments of Origin. Clay and Clay Minerals 24 107–113 and 114–117.
Lemaitre, R.W., 1989. A Classification of Igneous Rocks and Glossary of Terms. Blackwell, Oxford. 153 pp.
Lesta, P., Ferello, R., 1972. Region extraandina de Chubut y norte de Santa Cruz. In: Leanza, A.F. (Ed.), 1st Symp. Regional Geology of Argentina, Academia Nacional de Ciencias, Córdoba, Argentina, pp. 601–653.
Logan, V., Garrido, L., Etcheverry, R., 1992. Consideraciones geológicas, mineralógicas y tecnológicas de algunos depósitos de caolín del Departamento Gaiman, Chubut, Argentina. Actas IV Congreso Nacional y I Congreso Latinoamericano de Geología Económica. Córdoba, pp. 538–541.
Maiza, P., Hayase, K., 1975. Los yacimientos de caolín de la Patagonia. República Argentina. II Congreso Ibero-Americano de Geología económica, pp. 326–384.
Malumián, N., 1983. Foraminíferos cretácicos de la Hoja 43 f. Chubut. Departamento de Investigaciones de Base del servicio Geológico Nacional. Inédito.
Malvicini, M., Llambias, E., 1974. Geología y génesis de depósitos de Manganeso de Arroyo Verde, provincia de Chubut. 5ª Congreso Geológico Argentino, Buenos Aires. Actas II, pp. 185–221.
Maniar, P.D., Piccoli, P.M., 1989. Tectonic discrimination of granitoids. Geological Society of American Bulletin 101, 635–645.
Marfil, S.A., Maiza, P.J., Cardellach, E., Corbella, M., 2005. Origin of kaolin deposit in the Los Menucos area (Río Negro province, Argentina). Clays Minerals 40, 283–293.
Murray, H., Keller, W., 1993. Kaolins, Kaolins and Kaolins. In: Murray, H., Bundy, W., Harvey, C. (Eds.), Kaolin Genesis and Utilization. Clay Mineral Society, Boulder, pp. 1–24.
Musacchio, E., Chebli, W., 1975. Ostrácodos no marinos y carófitas del Cretácico inferior en las provincias del Chubut y Neuquén. i. Ostrácodos y carófitas del Grupo Chubut. 2. Rayossoana quilimalensis nov. Gen., nov. Sp. De la Formación Rayoso, Neuquén. Ameghiniana XII (1), 70–96.
Nakamura, N., 1974. Determination of REE, Ba, Fe, Mg, Na, and K in carbonaceous and ordinary chondrites. Geochemistry and Cosmochemistry Acta 38, 757–775.
Nelson, C.E., 1988. Gold Deposits in the Hot Springs Environment. In: Schafer, R.W., Cooper, J.J., Vikre, P.G. (Eds.), Bulk Mineable Precious Metal Deposits of the Western United States. Symposium Proceedings. Geological Society of Nevada, pp. 417–432.
Nesbitt, H., Young, G., 1989. Formation and diagenesis of weathering profiles. Journal of Geology 97, 129–147.
Oliveri, J., Terrero, J., 1954. El yacimiento de material caolinico Don Emilio. Departamento Gaiman, Territorio del Chubut. Boletin — Dirección Nacional de Mineria 81.
Page, R., Ardolino, A., de Barrio, R., Franchi, M., Lizuaín, A., Page, S., Silva Nieto, D., 1999. Estratigrafía del Jurásico y Cretácico del Macizo de Somún Curá, provincias de Río Negro y Chubut. In: Caminos, R. (Ed.), Geología Argentina. Subsecretaría de Minería de la Nación. SEGEMAR: Instituto de Geología y recursos Minerales. Anales Nº 29, pp. 460–488.
Pothe de Baldis, D., 1976. Estudio palinilógico de las muestras de la hoja 44 g Cañadón Iglesias, Servicio Geológico Nacional. Inédito.
Pothe de Baldis, D., 1984. Microfloras Cenozoicas. En Geología y Recursos Minerales de la provincia de Río Negro. Relatorio 9ª Congreso Geológico Argentino, vol. 2 (4), pp. 293–411.
Ramos, V., Pesce, C., 1979. Metalogenesis de la Provincia del Chubut. Comentarios. Revista - Asociación Geológica Argentina XXXIV, 1.
Rapela, C., Pankhurst, R., 1993. El volcanismo riolítico del noreste de la Patagonia: Un evento meso-jurásico de corta duración y origen profundo. Actas del XII Congreso Geológico Argentino, Mendoza, vol. 4, pp. 179–188.
Roedder, E., 1977. Stable and metastable fluid inclusions data, Browns Canyon Fluospar District, Chafee Country, Colorado, and similar epithermal and hot springs deposits. Problems of ore deposition. 4th IAGOD Symposium, Varna, Bulgaria, vol. 2, pp. 186–195.
Romero, A., Dominguez, E., Wehell, R., 1975. Genesis de los yacimientos de caolin del río Chubut inferior. 2ª Congreso Iberoamericano de Geología Económica: Secretaría de Minería de Argentina, Buenos Aires, vol. 4, pp. 423–444.
Rubinstein, N., Gargiulo, M.F., 2005. Análisis textural de cuarzo hidrotermal del depósito El Pantanito, Provincia de Mendoza: nuevos aportes sobre su génesis. Revista de la Asociación Geológica Argentina 60 (1), 96–103.
Sacomani, L., Panza, J.L., 1998. Hoja Geológica 4366-III Las Plumas. Servicio Geológico y Minero Argentino. Instituto de Geología y Recursos Minerales.
Sakai, H., Matsubaya, O., 1977. Stable isotope studies of Japanese geothermal systems. Geothermics 5, 97–124.
Schalamuk, I.B., Zubia, M., Genini, A., Fernandez, R.R., 1997. Jurassic Epithermal Au–Ag Deposits of Patagonia, Argentina. : Ore Geology Reviews. Elsevier.
Schmidt, J.M., 1999. Weathering, Rainwater and Atmosphere Chemistry: Example and Modeling of Granite Weathering in Present Conditions in a CO_2 Rich, and in an Anoxic Palaeoatmosphere. In: Thiry, M., Simon-Coincon, R. (Eds.), Palaeoweathering, Palaeosurfaces and Related Continental Deposits. : Int. Ass. Sediment., vol. 27. Blackwell, London, pp. 21–41.
Schoen, R., White, D., Hemley, J., 1974. Argillization by descending acid of steamboat springs, Nevada. Clays and Clays Minerals 22, 1–22.
Shand, S., 1927. Eruptive Rocks. John Wiley & Sons, New York.
Sheppard, S., Gielg, H.A., 1996. Stable isotope geochemistry of clay minerals. Clay Minerals 31, 1–24.
Sillitoe, R., 1993. Gold-rich porphyry copper deposits: geological model and exploration implications. Special Paper — Geological Association of Canada 40, 465–478.
Sillitoe, R.H., 2004. Musings of future exploration targets and strategies in The Andes: Society of Economic Geologists. Special Publication, vol. 11. 1–14 pp.
Sillitoe, R.H., Cooper, C., Sale, M.J., Soechting, W., Echavarria, D., Galardo, J.L., 2002. Discovery and geology of the Esquel low-sulfidation epithermal gold deposit, Patagonia, Argentina: Society of Economic Geologists. Special Publication, vol. 9. 227–240 pp.
Simeone, R., Dilles, J.H., Paladino, G., Palomba, M., 2005. Mineralogical and stable isotope studies of kaolin deposits: shallow epithermal systems of western Sardinia, Italy. Economic Geology 100, 115–130.
Simpson, G., 1933. Statigraphic Nomenclature of the Early Tertiary of Central Patagonia. : Ann. Mus. Novit, vol. 644. New York.
Sotarello, G., Belvideri, J., Machuca, E., Castro de Machuca, B., 2002. Sistema epitermal de baja sulfuración en el area Casposo-Villa Corral, Calingasta, San Juan, Argentina. Argentina mining 2002, Mendoza, abstract, CD-Rom. 1 pp.
Spalletti, L., Mazzoni, M., 1977. Sedimentología del Grupo sarmiento en un perfil ubicado al sudoeste del lago Colgué Huapi, provincia del Chubut. Obra del Centenario del Museo de La Plata 4, 261–283.
Srodon, J., Eberl, D.D., 1987. Illite. In: Bailey, S.W. (Ed.), Reviews in Mineralogy, Micas: Mineralogical Society of America, vol. 13, pp. 495–544.
Stipanicic, P., Methol, E., 1972. Macizo de Somún Cura. In: Leanza, A. (Ed.), Geología regional Argentina, Academia Nacional de Ciencias. Córdoba, pp. 581–599.
Stoch, L., 1974. Mineraly Ilaste ("Clay Minerals"). Geological publishers, Warsaw. 186–193 pp.
Stoffegren, R., 1985. Genesis of acid-sulfate alteration and Au–Cu–Ag mineralization at Summitville, Colorado. Unpublished Ph. D. thesis, University of California (Berkeley), 204 pp.
Thiry, M., Schmitt, J.M., Simon-Coinçon, R., 1999. Problems, progress and future research concerning paleoweathering and paleosurfaces. International Association of Sedimentologist 27, 3–17.
Uliana, M., Biddle, K., Phelps, D., Gust, D., 1985. Significado del vulcanismo y extensión mesojurásicos en el extremo meridional de Sudamérica. Revista de la Asociacion Geologica Argentina 40 (3–4), 231–253.
Velde, B., 1999. In: Price, G.D., Ross, N.L. (Eds.), The Stability of Clays. Kluwer, The Netherlands, pp. 329–350.
Volkheimer, W., 1967. La paleoclimatología y los climas del Mesozoico argentino. Revista Minera, Geología y Mineralogía XXVIII-3, 41–48.
White, N., 1991. High-sulfidation of thermal gold deposits: characterization and a model for their origin. Geological Survey of Japan Rep. 227, 9–20.
Windhausen, A., 1921. Informe sobre un viaje de reconocimiento geológico en la parte nordeste del Territorio del Chubut, con referencia especial a la cuestión de provisión de agua de Puerto Madryn: Dirección General de Minas, Geología e Hidrogeológia, Boletín, vol. 24, pp. 1–72. serie B.
Yllanes, E., 1979. Descripción geológica de la Hoja 42g, Telsen, Servicio Geológico Nacional. Inédito.
Zubia, M.A., Genini, A.D., Schalamuk, I.B., 1999. Yacimiento Cerro Vanguardia, Santa Cruz: Instituto de Geología y Recursos Minerales SEGEMAR [Buenos Aires]. Anales 35, 1189–1202.